Assimilation overwhelms nitrification in saline wastewater nitrogen removal

From heterotrophic nitrification and aerobic denitrification strains to microbiomes

Zhang, Mengru; Zhang, Wenhao; Jiang, Qingyuan; Zhao, Chuanfu; Han, Fei; Chen, Hao; Li, Yuke; Zhuge, Yuping; Zhou, Weizhi

DOI
10.1016/j.watres.2025.124694

Publication date
2025

Document Version
Final published version

Published in
Water Research

Citation (APA)
Zhang, M., Zhang, W., Jiang, Q., Zhao, C., Han, F., Chen, H., Li, Y., Zhuge, Y., & Zhou, W. (2025). Assimilation overwhelms nitrification in saline wastewater nitrogen removal: From heterotrophic nitrification and aerobic denitrification strains to microbiomes. *Water Research*, *288*, Article 124694. https://doi.org/10.1016/j.watres.2025.124694

Water Research 288 (2026) 124694

Contents lists available at ScienceDirect

Water Research

journal homepage: www.elsevier.com/locate/watres

Assimilation overwhelms nitrification in saline wastewater nitrogen removal: From heterotrophic nitrification and aerobic denitrification strains to microbiomes

Mengru Zhang [a,b], Wenhao Zhang [a,b], Qingyuan Jiang [a,b], Chuanfu Zhao [a,b], Fei Han [a,b], Hao Chen [a,b], Yuke Li [c], Yuping Zhuge [d], Weizhi Zhou [a,b,*]

[a] School of Civil Engineering, Shandong University, 250061 Jinan, China
[b] Laboratory of Water-Sediment Regulation and Eco-decontamination, 250061, Jinan, China
[c] Department of Water Management, Faculty of Civil Engineering and Geosciences, Delft University of Technology, Stevinweg 1, 2628 CN Delft, the Netherlands
[d] College of Resources and Environment, Shandong Agricultural University, 271018, Taian, China

HIGHLIGHTS

- Two heterotrophic nitrification and aerobic denitrification strains are isolated.
- Nitrogen metabolic pathways are identified in two halophilic strains.
- Microbiomes with distinct nitrogen metabolism are constructed by HN-AD strains.
- Biofilm-forming strains facilitate the deterministic assembly of microbiomes.
- Ammonium assimilation overwhelms nitrification in microbiomes.

GRAPHICAL ABSTRACT

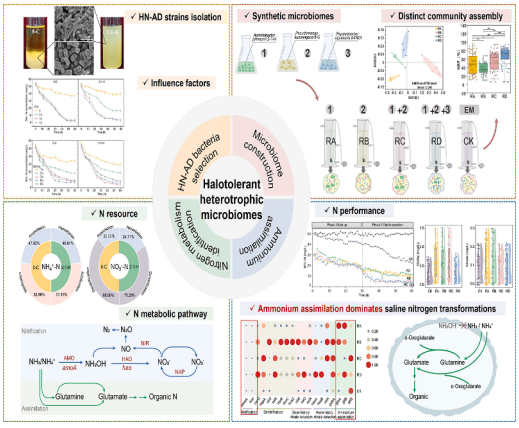

ARTICLE INFO

Keywords:
Heterotrophic nitrification and aerobic denitrification
Synthetic microbiome
Heterotrophic halophilic microbiome
Ammonium assimilation
Saline wastewater treatment

ABSTRACT

Heterotrophic nitrification and aerobic denitrification (HN-AD) represents an innovative biological nitrogen removal strategy for saline wastewater treatment. However, how HN-AD microbes could be applied to environmental microbiomes and conduct nitrogen metabolic performance remains ambiguous. Here we established synthetic heterotrophic microbiomes using halophilic HN-AD strains - biofilm-forming *Pseudomonas kunmingens* 8-C and *Acinetobacter johnsonii* 2–1-H, and characterized nitrogen metabolism in pure-cultured strains and microbiomes. The pure-cultured HN-AD strains removed ammonium primarily via ammonium assimilation (> 46 % contribution) and heterotrophic nitrification, comprehensively validated by nitrogen balance, ^{15}N stable isotopic labeling tests, enzyme activity assays and functional gene identification. Four synthetic halophilic microbiomes constructed by biofilm-forming and HN-AD strains achieved ammonium and total nitrogen removal

* Corresponding author.
E-mail address: wzzhou@sdu.edu.cn (W. Zhou).

https://doi.org/10.1016/j.watres.2025.124694
Received 4 July 2025; Received in revised form 25 September 2025; Accepted 27 September 2025
Available online 27 September 2025

efficiencies of 76-92 % and 72–86 %. Biofilm-forming strains facilitated heterotrophic microbiome assembly by shaping microbial communities through the deterministic assembly process. Notably, initial functional strains selectively recruited environmental microbes with efficient ammonium-assimilating capacity, manifested as a stable and relatively high abundance of *glnA* gene in microbiomes. But the invasion of microbes consequently led to the overwhelming dominance of ammonium assimilation over nitrification in microbiomes. Our results provided a framework for constructing environmental microbiomes using functional microbes and highlighted the distinct nitrogen metabolism shifting from HN-AD pure-cultured bacteria to microbial consortia.

1. Introduction

The industry expansion and extensive seawater utilization in anthropogenic activities lead to the increasing discharge of saline wastewater. Saline wastewater is usually generated from various industries such as seafood processing, petrochemical, pharmaceuticals and marine aquaculture, and typically contains salinity levels ranging from 15 to 45 g/L (Srivastava et al., 2021). Saline wastewater poses detrimental effects on existing biological treatment processes, potentially leading to the discharge of nitrogenous contaminants and resultant water quality deterioration. Conventional nitrification process in biological nitrogen removal (BNR) is particularly inhibited by salinity, leading to the inevitable accumulation of intermediate and decline in nitrogen removal performance (Corsino et al., 2019; Li et al., 2023). Compared to ammonia-oxidizing bacteria (AOB) and nitrite-oxidizing bacteria (NOB) carrying out nitrification dominating freshwater treatment systems, autochthonous halophilic microbes possess advantages of salinity tolerance and robust biological metabolism. Heterotrophic nitrogen removal carried out by halophilic bacteria is more favorable in saline environments benefiting from the stronger resistance to osmotic stress and environmental fluctuations (Qiang et al., 2023), presenting a promising approach for BNR in saline wastewater (Ke et al., 2025; Zhang et al., 2021).

Heterotrophic nitrification and aerobic denitrification (HN-AD) microbes have been explored as promising candidates for BNR due to their fast growth rate and versatile metabolic activities (Wu et al., 2024). Particularly in saline environments, halophilic HN-AD microbes have achieved efficient nitrogen removal at salinity exceeding 3 % (Huang et al., 2023; Xu et al., 2024). However, nitrogen transformations in HN-AD pathway remain incompletely understood, particularly due to the fragmented knowledge of genes and enzymes associated with heterotrophic ammonia oxidization (Lenferink et al., 2024; Xi et al., 2022). At phenotypic level, the nitrification pathway in HN-AD is generally presumed to occur through a similar mechanism as in typical nitrifiers (Martikainen 2022), involving the stepwise conversion of ammonia to dinitrogen gas via hydroxylamine, nitrite, nitric oxide and nitrous oxide as intermediates. Ammonium assimilation (AA) serves as the other primary nitrogen removal pathway in most HN-AD bacteria, which accounts for half and even more of the total nitrogen removal flux (Hu et al., 2024; Huang et al., 2023; Wei et al., 2025; Xie et al., 2023). At genetic level, classical functional genes involved in traditional autotrophic nitrification (*amoA* and *hao*) have been reported to be missing in HN-AD strains (Cui et al., 2021), and new molecular markers (*haoA, haoB* and *haoC*) involved in the conversion of hydroxylamine to nitrite have been recently used to represent the characteristic process of HN-AD (Yang et al., 2025). Therefore, elucidating nitrogen transformations in the physiology of HN-AD is critical for its accurate applications and effective regulation strategies.

The application of HN-AD to BNR in saline wastewater treatment has gained increasing attention, owing to its advantage of simultaneous nitrogen transformations in a single unit under aerobic conditions and the resultant reduction of investment costs and operational complexity (Cui et al., 2021). The application of functional microbes to open environmental systems faced practical challenges. Current approaches to establish mature HN-AD biosystems and optimize intensified performance were still time-consuming via the bioaugmentation of pure-cultured HN-AD bacteria into membrane bioreactors every 2–3 days for at least 10 days (Lan et al., 2023; Ren et al., 2021), or limited to sterilized solution (Huang et al., 2020). Fortunately, the “bottom-up” design of synthetic microbiomes, referring to the utilization of selected microbes to optimize synergistic performance (Ruan et al., 2024), enables the construction of desired microbiomes with improved efficiency and functional complexity from the pre-cultured functional microbes (Lawson et al., 2019). Biofilms existing as bioflocs and particles in wastewater treatment systems could provide stabilized habitats (Shi et al., 2024), and these spatial structures successfully help functional microbes cross the gap from the pure culture to ammonium-assimilating microbiome under saline condition (Zhang et al., 2021). However, building synthetic microbiomes may easily failed because of the susceptibility to invasion by naturally occurring microbes (Lawson et al., 2019). Provided that biofilm-forming capability could help maintain functional and structural stability of microbial communities, the fact that HN-AD possesses both ammonia nitrogen nitrification and assimilation metabolic pathways makes the nitrogen metabolism in microbiomes ambiguous. It has been currently reported that nitrification is gradually replaced by heterotrophic assimilation with the increase of carbon to nitrogen ratio (C/N) (Lenferink et al., 2024). Consequently, understanding the nitrogen metabolism of HN-AD microbes and the complex microbial interactions during microbiome construction could shed light on providing engineering strategies for applying functional microbes to environmental microbiomes.

In our previous study, heterotrophic marine bacteria with capability of biofilm formation have been screened from seafloor sediment samples collected at A4 (122°48′ E, 35°59′ N) in the Yellow Sea (Zhang et al., 2021). Taking advantage of these heterotrophic microbial resources, this study aimed to (i) isolate and identify HN-AD strains with high salt tolerance and robust nitrogen metabolism; (ii) uncover the nitrogen conversions in HN-AD bacteria based on genetic characteristics, phenotypic analysis and specific enzyme activities; (iii) construct microbiomes with functional HN-AD bacteria in saline wastewater and evaluate their nitrogen metabolism. Accordingly, two HN-AD strains were investigated and a promising method for application of functional microbes into microbial consortia was provided.

2. Materials and methods

2.1. Isolation and metabolic characteristic analysis of HN-AD bacteria

The components of the medium used in this study were provided in Table S1, including the marine Luria-Bertani (LB) medium, bromothymol blue (BTB) medium, heterotrophic nitrifying screening medium (HNM), and aerobic denitrifying screening medium (DEM). The cultivation methods of strains were detailed provided in Text S1 in Supplementary material.

The screening of HN-AD functional microbes was based on blue ring selection in BTB solid medium and rapid bacteria growth, while detailed screening steps were provided in Text S1. After inoculating in HNM, eight strains with OD_{600} higher than 0.6 were selected for their rapid growth. The secondary isolation was based on NH_4^+-N and NO_3^--N removal efficiencies in HNM and DEM after cultivation for 24 h (Fig. S1). Strain 8-C and 2–1-H were selected for subsequent study due to their efficient nitrogen removal performance and biofilm-forming function of

8-C.

The morphological and biochemical characteristics of two targeted strains were measured after inoculation in LB media for 48 h. The biomass in the flask was measured every 3 h to draw growth curves of strains 2–1-H. Since the strain 8-C could form sedimentary biofilms during cultivation, the dry cell weight was calculated instead of OD_{600} to represent the bacterial growth (Huang et al., 2018).

2.2. Molecular analyses

To identify two screened HN-AD strains, 16S rRNA genes were amplified and then analyzed by electrophoresis and sequenced by Major Biotech (Shanghai, China) Co., Ltd. The obtained nucleotide sequence was compared online by Basic Local Alignment Search Tool (BLAST) method. The phylogenetic tree was performed in MEGA 7.0 program by the neighbor-joining method with bootstrap values of 1000 replications. The genomes of two selected strains were also extracted and sequenced using an Illumina HiSeq 4000 system (Illumina, San Diego, CA, USA) at Major Biotech (Shanghai, China) Co., Ltd. The best hit abstracted using Blast alignment tool for functional annotation. The evaluation of classical nitrification (*amo* and *hao*) and heterotrophic nitrification (*haoA, haoB* and *haoC*) functional genes were using previously published primers and methods (Table S2).

2.3. Nitrogen metabolism of HN-AD strains

2.3.1. Nitrogen conversions in HN-AD strains

Strain 2–1-H and 8-C cultured for 24 h in LB medium were collected, washed and then inoculated into different media. HNM and DEM were prepared to investigate HN-AD activity of strains by using 50 mg/L of initial ammonium or nitrate as the sole nitrogen source, respectively. Since organic matter was a necessary source of nutrients and energy for the growth and reproduction of heterotrophic microbes, the C/N ratio (referring to the chemical oxygen demand to total nitrogen ratio) of 10 was used. Samples were withdrawn from the flasks periodically to determine NH_4^+-N, NO_2^--N, NO_3^--N, total nitrogen (TN) and Intracellular-N. The calculation formulas of proportions of nitrification/denitrification and ammonium assimilation in HN-AD process were provided in Supplementary material.

2.3.2. ^{15}N stable isotopic labeling tests

Stable isotope tests with ^{15}N were conducted to identify the nitrogen transformation during the HN-AD reactions of strains 2–1-H and 8-C. $^{15}NH_4^+$ was used in the form of $^{15}NH_4Cl$ (Shanghai Macklin Biochemical Co., Ltd, China, with 10 atom % ^{15}N). Bacterial cells cultivated in LB medium were collected and washed with the fresh PBS buffer to remove residual medium. Samples were taken from the systems after incubation to measure the concentrations of NH_4^+-N in supernatant, TN in biomass and gaseous nitrogen. Gaseous samples were collected with tinfoil gas collecting bag to determine the concentrations of gaseous N_2O and N_2. The levels of $^{15}N_2O$ and $^{15}N_2$ present in the headspace were measured by GC–MS (Agilent, USA) and GC-RMS (Thermo Fisher Scientific, USA), respectively.

The relative ^{15}N isotopic abundance ($\delta^{15}N$) of a sample was calculated by equation showing below (Denk et al., 2017; Mariotti 1983).

$$\delta^{15}N = \frac{atom\%^{15}N(sample) - atom\%^{15}N(air)}{atom\%^{15}N(air)} \times 1000$$

where the ^{15}N isotopic ratio in the air is 0.3663 %. The $\delta^{15}N$ ratio of N_2 and N_2O were more than zero, indicating that ^{15}N-labelled gas was produced and released.

2.3.3. Key enzymes activity detection

The activities of enzymes related to HN-AD were determined in two strains. AMO (ammonia monooxygenase), HAO (hydroxylamine oxidase), HAP (nitrate reductase) and NIR (nitrite reductase) catalyzed reactions from ammonia nitrogen to hydroxylamine, hydroxylamine to nitrite, nitrate reacting to nitrite and the reduction of nitrite to nitrogenous gas, respectively. BCA protein assay kit (Solabio, China) was used to measure the protein concentration in the crude enzyme solution. The specific operation steps were carried out in accordance with the instructions of the assay kit.

2.4. Effects of different factors on ammonium removal performance

The HN-AD efficiencies of strains 2–1-H and 8-C were evaluated under different conditions of carbon to nitrogen (C/N), salinity, carbon sources, temperature and pH values. The C/N ratios referred to the chemical oxygen demand (COD) to TN ratio in this study. Sodium acetate, sodium succinate, glucose and sucrose were respectively added to the HNM as carbon sources to establish a C/N ratio of 10. Different initial C/N ratios (5, 7.5, 10, 15) were controlled by adjusting the concentration of sodium acetate as carbon source. The effect of salinity on ammonium removal was conducted by adjusting NaCl concentrations to salinity of 1 %, 2 %, 3 %, 5 % and 8 % (w/v) in HNM. Initial pH values of HNM were adjust to 5, 6, 7, 8 and 9 for the effect of pH. Strains were cultivated under temperature at 15, 20, 25 and 30 °C. Time-series samples of NH_4^+-N concentration were measured to reflect ammonium removal performance. Cell density or dry weight of strains were measured to reveal the effect on growth.

2.5. Construction and operation of HN-AD microbiomes

2.5.1. Construction of microbiomes

Column-type sequential batch reactors (SBRs) with unsterilized synthetic wastewater were used to develop HN-AD microbiomes. The detailed dimensions of SBRs referred to our previous study (Zhang et al., 2021). Operation settings of SBRs were set with 12 h per cycle that consisted of 5 min feeding, 690 min aeration, 15 min settling and 10 min decanting. Air was supplied through an aeration pump with the dissolved oxygen controlled at about 5.0–6.5 mg/L. The synthetic high saline wastewater contained (per liter): 960 mg (in startup phase with C/N ratio of 15) or 1280 mg (in stable phase with C/N ratio of 20) sodium acetate; 190 mg NH_4Cl; 40 mg KH_2PO_4; 33 g seawater crystal. Salinity used in this study was determined based on the average value of salinity in saline wastewater and the salinity of real seawater.

Four microbiomes were built in bioreactors (namely RA, RB, RC and RD) with strain 8-C, strain 2–1-H, strains 2–1-H and 8-C with the ratio of 1:1 (v/v), and two HN-AD strain and ammonium-assimilating strain *Psychrobacter aquimaris* A4N01 with the ratio of 1:1:1 (v/v), respectively. The bioreactor (RB) was filled with 30 % (v/v) cylindrical fillers (K2, plastic media with a diameter and height of 15 and 10 mm) as biofilm carriers. Strains were firstly cultured in LB medium and then inoculated into synthetic saline wastewater with an initial mixed liquor suspended solid (MLSS) of 2 g/L in each reactor. In start-up phase, reactors were operated with a 24-h cycle for microbiomes to form settleable flocs and to acclimate to the environment for 10 days. For comparison, a control system (CK) was operated under the identical operating parameter without the inoculation of any microbes.

2.5.2. Sludge properties of microbiomes

Extracellular polymeric substance (EPS) of each microbiome was extracted by heat method (Zhang et al., 2016). Concentrations of proteins (PN) and polysaccharides (PS) in EPS were detected using the modified Lowry method (Lowry et al., 1951), and phenol-sulfuric acid method (DuBois et al., 1956), respectively. Three-dimensional excitation-emission matrix (3D-EEM) analysis of EPS was conducted and further analyzed using Parallel Factor Analysis (PARAFAC) in MATLAB 2018 (MathWorks, Natick, MA, USA) according to previous study (Zhao et al., 2023).

2.6. Microbial community analysis

Microbial samples from each reactor were collected at 5, 10, 30, 50, 60 days during the process of microbiome construction and sent to Majorbio BioPharm Technology Co., Ltd. (Shanghai, China) for PCR amplification (the V3-V4 region of 16S rRNA) and high-throughput sequencing (Miseq illumina platform).

Co-occurrence network analysis was conducted to explore the coexistence of bacterial taxa by calculating Spearman's rank correlation coefficient matrix based on the relative abundance of bacterial OTU using R v4.3.3. The occurrence networks were then visualized with Gephi software (0.10). The normalized stochasticity ratio (NST) index was calculated based on the OTU abundance matrix to determine the extent of stochasticity in microbial community assembly processes. The higher values (NST >50 %) and lower values indicated greater influence of stochastic processes and more deterministic process, respectively (Ning et al., 2019). The aggregatesR package (https://github.com/Github-Yilei/aggregatesR/blob/master/R/ternary_plot.R) was used to conduct the ternary plot analysis.

Genomic DNA samples of microbiomes were extracted using the FastDNA SPIN Kit for Soil (MP Biomedicals, America). Nitrogen functional genes were quantified from genomic DNA using qPCR (qTOWER3 G, Analytic Jena AG, Germany). Primers used in qPCR were provided in Table S2.

2.7. Analytical methods and statistical analysis

The scanning electron microscope (SEM) analysis (JEOL JSM-7600F, Japan) of microbial cells was conducted according to previous work to observe cellular structure (Huang et al., 2018). The concentrations of NH_4^+-N, NO_2^--N, NO_3^--N, and total nitrogen (TN) were measured with spectrophotometer according to standard methods. The concentration of hydroxylamine was determined spectrophotometrically at 705 nm using matched 1 cm Corex cuvettes. Intracellular-N content was the TN of inoculated media minus TN of inoculated media following centrifugation. The data were calculated and plotted by Origin 2024 software. Differences among groups were analyzed with SPSS 24.0. The p value < 0.05 was considered significant.

3. Results

3.1. Isolation and identification of functional bacteria

Two strains exhibiting the highest ammonium and nitrate removal efficiencies were selected after incubated in HNM and DEM medium. Strains 8-C and 2–1-H shared the highest identity with *Pseudomonas kunmingens* and *Acinetobacter johnsonii*, respectively (Fig. 1a and b). SEM analysis revealed the long rod shapes of strain 8-C and short rod shapes of 2–1-H (Fig. 1c). Notably, strain 8-C showed the floc-forming capability and auto-aggregation in liquid medium, which could benefit in effective settleability and biomass retention during microbiome assembly. Both strains exhibited robust growth under saline conditions, as evidenced by their growth curves (Fig. 1d). Strain 8-C achieved the maximum dry weight of biomass of 1.5 g/L after 24 h, while strain 2–1-H reached an OD_{600} of 2.10 after 48 h cultivation. Based on the rapid growth of strain 2–1-H and the excellent self-flocculation performance

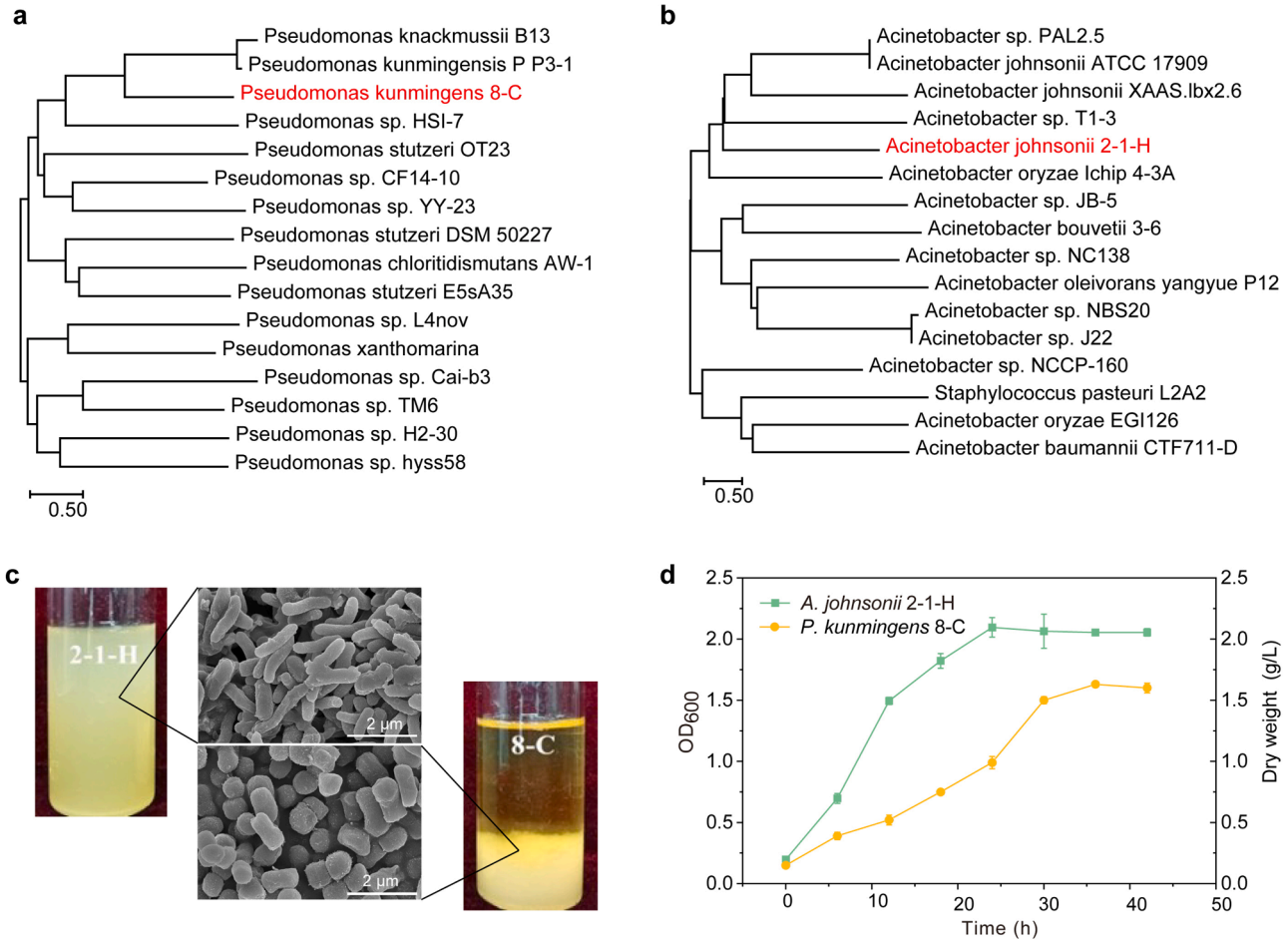

Fig. 1. Identification, morphology and growth curves of two strains. a,b Phylogenetic trees derived from neighbor-joining analysis of partial 16S rDNA sequences. c, The micromorphology of strains in fluid media and under scanning electron microscope (SEM). d, Growth curves of strains 2–1-H and 8-C.

of strain 8-C, the two strains were studied simultaneously.

3.2. Nitrogen transformations of HN-AD strains

3.2.1. Nitrogen removal through heterotrophic nitrification

The heterotrophic nitrification capability of strains 8-C and 2–1-H was evaluated in HNM with ammonium as the sole nitrogen source (Fig. 2a-d). Strain 8-C exhibited rapid NH_4^+-N removal with concentration declining sharply from initial 54.2 mg/L to 2.9 mg/L in the first 48 h, the NH_4^+-N removal efficiency of 94.6 % and the average ammonium removal rate of 2.1 mg/N·L^{-1}·h^{-1} in 24 h. In strain 2–1-H, 89.1 % of initial NH_4^+-N was removed with the NH_4^+-N removal rate of 1.88 mg/N·L^{-1}·h^{-1} in 24 h and the residual NH_4^+-N concentration of 5.5 mg/L. The ammonium removal process was accompanied by the rapid growth of microbial biomass, demonstrated by increasing dry weight of the strain 8-C and OD_{600} values of strain 2–1-H. Both strains demonstrated efficient ammonium removal performance comparable to reported HN-AD bacteria (Hu et al., 2024; Huang et al., 2023; Lan et al., 2023). Neither strain showed NO_2^--N accumulation during the heterotrophic nitrification process. Transient NO_3^--N accumulation was observed in both strains at 30 h with the final residual NO_3^--N stabilizing at approximately 4 mg/L after 48 h, consistent with some other HN-AD bacteria (Zhang et al., 2017). The accumulation of nitrate and subsequent consumption probably resulted from the aerobic denitrification process or assimilation of nitrate.

Nitrogen transforming balance (Fig. 2b and Table S3) and ammonium transforming flux calculations (Fig. 2c) demonstrated nitrogen metabolic pathways of strains. Obvious nitrogen loss in systems was observed in the total nitrogen balance analysis, indicating the production of gaseous nitrogen. Up to 96.2 % and 89.1 % of the supernatant TN was removed by the strain 8-C and 2–1-H, respectively. In strain 8-C, 50.1 % of the initial TN was finally converted into gaseous nitrogen,

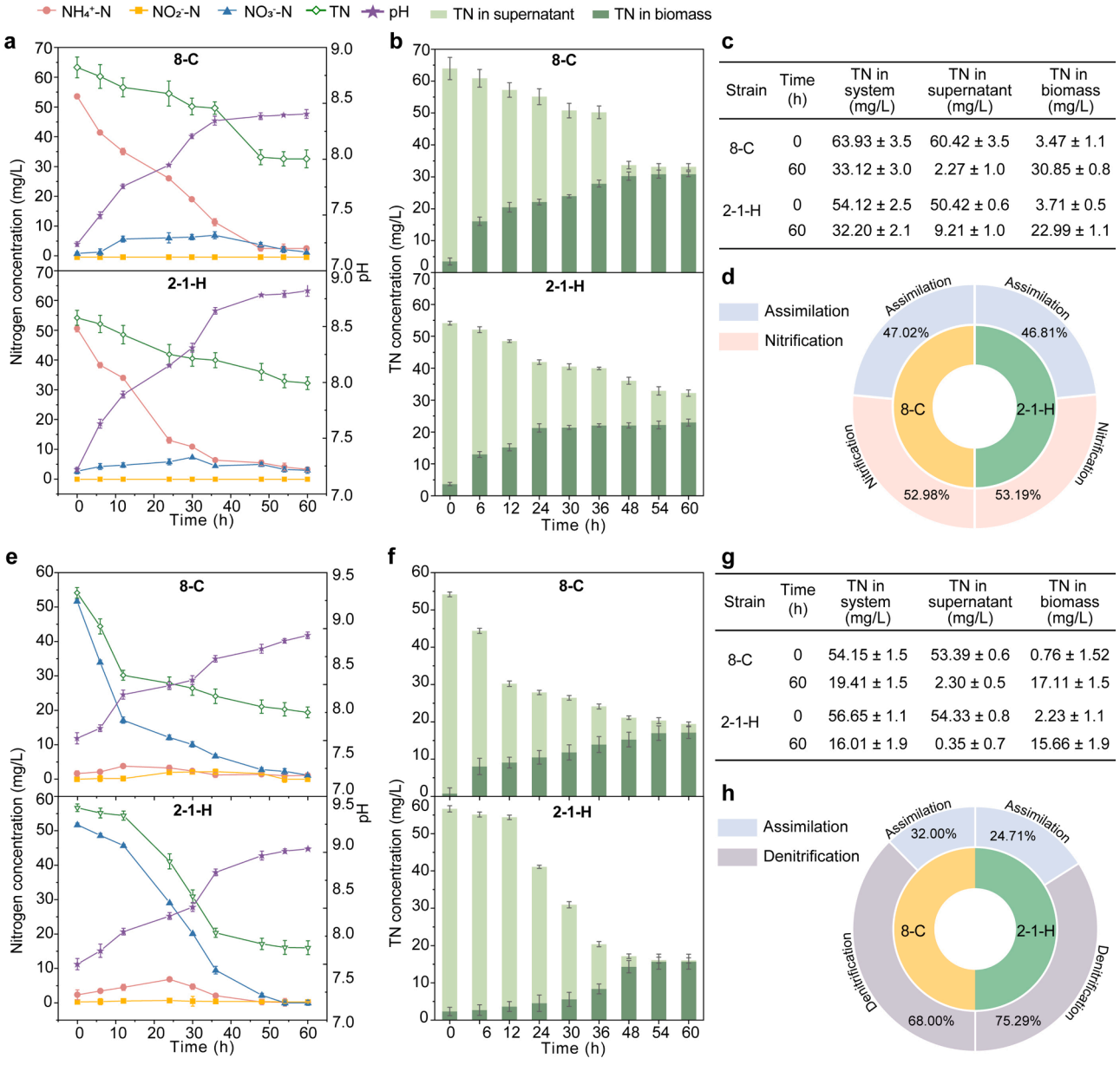

Strain	Time (h)	TN in system (mg/L)	TN in supernatant (mg/L)	TN in biomass (mg/L)
8-C	0	63.93 ± 3.5	60.42 ± 3.5	3.47 ± 1.1
	60	33.12 ± 3.0	2.27 ± 1.0	30.85 ± 0.8
2-1-H	0	54.12 ± 2.5	50.42 ± 0.6	3.71 ± 0.5
	60	32.20 ± 2.1	9.21 ± 1.0	22.99 ± 1.1

Strain	Time (h)	TN in system (mg/L)	TN in supernatant (mg/L)	TN in biomass (mg/L)
8-C	0	54.15 ± 1.5	53.39 ± 0.6	0.76 ± 1.52
	60	19.41 ± 1.5	2.30 ± 0.5	17.11 ± 1.5
2-1-H	0	56.65 ± 1.1	54.33 ± 0.8	2.23 ± 1.1
	60	16.01 ± 1.9	0.35 ± 0.7	15.66 ± 1.9

Fig. 2. Performance of nitrogen transformations by *A. johnsonii* 2–1-H and *P. kunmingens* 8-C. a, Ammonium transformation. b, Changes of total nitrogen (TN) between the supernatant and biomass during ammonium transformations. c, Balances of TN during ammonium transformations. d, Conversion proportions of assimilation and nitrification. e, Nitrate transformation. f, Changes of total nitrogen (TN) between the supernatant and biomass during nitrate transformations. g, Balances of TN during nitrate transformations. h, Conversion proportions of assimilation and denitrification.

and 3.8 % of TN was accumulated as nitrification intermediates in supernatant. In strain 2–1-H, 43.5 % of the initial nitrogen was assimilated into intracellular-N, while 18.3 % was accumulated as intermediates. Consequently, ammonium assimilation accounted for 47.0 % and 46.8 % of the heterotrophic ammonium removal in strains 8-C and 2–1-H, respectively. Both strains exhibited progressive pH elevation during ammonium removal, likely resulted from the utilization of organic matter during heterotrophic microbial growth (Zhang et al., 2022). Additionally, the relatively stable pH values in strain 8-C (from 7.2 to 8.4) compared to strain 2–1-H might reflect the biofilm-mediated buffering effects.

3.2.2. *Nitrogen removal through aerobic denitrification*

To assess the aerobic denitrification performance, strains 8-C and 2–1-H were aerobically cultivated in DEM with nitrate as the sole nitrogen source (Fig. 2e-h). After 48 h incubation, 94.6 % of NO_3^--N removal rate was achieved in strain 8-C with an average NO_3^--N removal rate of 4.2 mg/N·L^{-1}·h^{-1}, while 95.7 % of NO_3^--N were removed by the strain 2–1-H with the average NO_3^--N removal rate of 4.24 mg/N·L^{-1}·h^{-1}. The average NO_3^--N removal rate for the strains 2–1-H and 8-C were equivalent and even higher than reported HN-AD bacteria with 3.63–4.63 mg/(L·h) (Cui et al., 2021; Wei et al., 2025). In addition, transient nitrite accumulation and slight pH variations occurred (< 2.2 mg/L) during aerobic denitrification, consistent with previous studies (Zhang et al., 2017).

Throughout nitrate removal, the decrease of TN concentration in supernatant was basically consistent with the change of nitrate concentration in both strains 8-C and 2–1-H (Fig. 2f). Up to 64.1 % and 71.7 % of the supernatant TN was removed by the strain 8-C and 2–1-H, respectively. Nitrogen balance analysis revealed that 32.0 % and 24.7 % of the removed nitrogen was assimilated into intracellular-N in strain 8-C and 2–1-H, respectively. Denitrification of nitrate to gaseous nitrogen represented 68.0 % and 75.3 % of the TN removal in strain 8-C and 2–1-H, respectively. Results demonstrated that the conversion of nitrate to intracellularly ammonium by assimilatory nitrate reduction contributed significantly to nitrogen removal of nitrate in HN-AD bacteria.

a

Sample	Time (h)	NH_4^+-N		N_2O	N_2	^{15}N isotopic ratios in biomass (%)
		^{15}N isotopic ratios (%)	Content (mg/L)	$\delta^{15}N$ (‰)	$\delta^{15}N$ (‰)	
Acinetobacter johnsonii 2-1-H	0	2691.47	57.4	-	-	0
	10	1149.15	24.5	11.207	139.900	206.67
Pseudomonas kunmingens 8-C	0	2706.06	50.8	-	-	0
	10	1060.45	26.8	3.3055	138.359	204.72

b

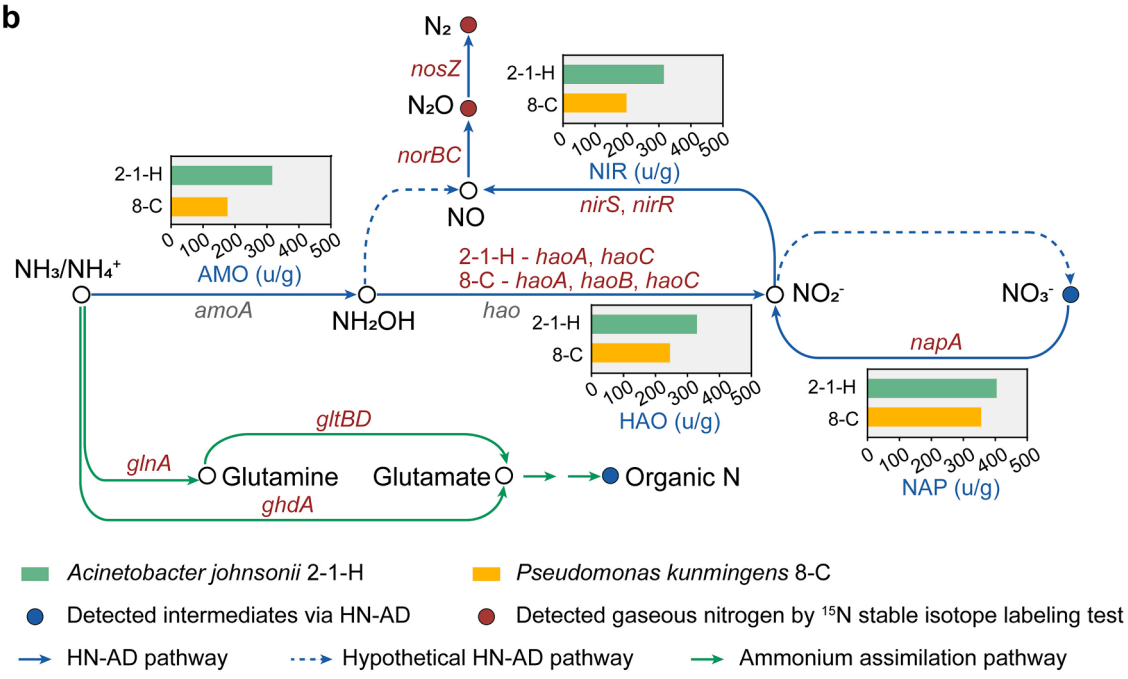

Fig. 3. Speculative nitrogen transformations of strains 2–1-H and 8-C. a, ^{15}N stable isotope labeling test under aerobic condition. b, Nitrogen metabolic pathway of strain 2–1-H and 8-C. AMO, ammonia monooxygenase; HAO, hydroxylamine oxidase; HAP, nitrate reductase. Undetected functional nitrogen genes were represented in grey, while detected functional genes were represented in red.

3.2.3. Nitrogen removal mechanisms of strains 2–1-H and 8-C

Nitrogen functional genes detected in genomes of strain 8-C and 2–1-H were shown in Table S4. Both strains contained genes coding for complete aerobic denitrification and assimilatory nitrate reduction pathway. The periplasmic nitrate reductase and nitrite reductase, coding by genes *nap*A and *nir*S respectively, have been reported to play indispensable roles in high oxygen tolerance and aerobic denitrification process (Xu et al., 2025). Functional genes associated with classic autotrophic nitrification, including *amoA* (encoding ammonia monooxygenase) and *hao* (encoding hydroxylamine dehydrogenase) were failed to detect in genomes in both strains. The existence of *amo*A and *hao* genes that were amplified by qPCR with specific primers provided theoretical support for their heterotrophic nitrifying capability, but the high Ct values indicated the low abundance of nitrifying genes (Table S5). The discrepancy between missing classical *amo*A and *hao* genes in genomes but the presence in qPCR detection might result from the incomplete sequencing of the whole genomes, or primers bias toward ammonia monooxygenase (AMO) of chemolithotrophic nitrifiers rather than that of heterotrophic nitrifiers. To further verify the heterotrophic nitrification at the genetic level, recently reported molecular markers (*haoA, haoB* and *haoC*) were amplified (Yang et al., 2025). Genes *haoA* and *haoC* were detected in strain 8-C and 2–1-H, while *haoB* was only detected in strain 8-C (Table S5). The absence of *haoB* in 2–1-H might be due to the specificity of the strain, and thus further verification might be required for the universality of these new molecular markers.

The ^{15}N stable isotope labeling test demonstrated gaseous nitrogen production in two strains that ^{15}N labeled $^{15}N_2O$ and $^{15}N_2$ were detected during HN-AD process (Fig. 3a). The detection of ^{15}N in biomass confirmed the cellular ammonium assimilation. The isotopic labeling test proved that both nitrification and assimilation contributed to nitrogen removal in these strains. It was preliminarily concluded that ammonium was oxidized to NH_2OH and then converted to gaseous nitrogen in HN-AD pathway: NH_4^+-N → intermediates → N_2O → N_2. Key enzyme activities of AMO, HAO, HAP and NIR verified the presence of nitrification and denitrification in the crude enzyme extracts of both strain 8-C and 2–1-H, though the activity values of the key enzymes differed between the two strains (Fig. 3b). Although conventional *hao* genes were not detected, the function of converting hydroxylamine into nitrite and amplification of heterotrophic hao-like genes confirmed heterotrophic nitrification.

The HN-AD pathways were depicted in Fig. 3b by summarizing the results of genome analysis, ^{15}N stable isotope labeling test, amplification of key genes, and enzyme activities. In recent study, direct ammonium oxidation to dinitrogen gas did not occur in HN-AD bacteria confirmed by the detect of ^{15}N labeled NH_2OH in isotope test (Lenferink et al., 2024). Considering the detection of ammonium oxidation and hydroxylamine oxidation activity as well as hao-like genes, the speculative HN-AD pathways in strains 8-C and 2–1-H were assumed as NH_4^+-N → NH_2OH → nitrogenous gas or/and NH_4^+-N → NH_2OH → NO_2^--N → NO_3^--N→ NO_2^--N → nitrogenous gas.

3.3. Construction and performance of heterotrophic microbiomes

3.3.1. Nitrogen removal performance of microbiomes

Benefiting from stress tolerance and metabolic adaptability to various environmental conditions including carbon sources, salinity, carbon to nitrogen ratios and pH (Text S2 in Supplementary material), heterotrophic microbiomes were established by inoculating HN-AD strains involved with environmental microbes. The biofilm-forming strain 8-C served as the foundational microbe for the microbiome assembly of RA. To maintain biomass of functional microbes, strain 2–1-H were cultivated immobilized on cylindrical fillers (RB) and with biofilm-forming strain 8-C (RC). The self-flocculating bacteria *Psychrobacter aquimaris* A4N01 was also added to improve biofilm formation for HN-AD bacteria to maintain biomass (RD). The role of ammonium-assimilating strain A4N01 has been well-studied that it played as the key taxon to provide biofilms and initial nitrogen metabolism by selectively enriching heterotrophic environmental microbes during microbiome assembly (Zhang et al., 2021). A control system (CK) without initial HN-AD bacteria was operated in parallel to monitor indigenous development of environmental microbes during microbiome construction.

Attributed to the biofilm-forming capability of strain 8-C and strain A4N01, flocs formed rapidly in microbiomes RA, RC and RD. The fillers in RB also provided niches for microbes to reproduce and accumulate biomass (Fig. S3a). As a result, NH_4^+-N removal efficiencies gradually reduced within 30 days of the start-up phase (Fig. 4a), with average efficiencies of 54.1 ± 4.5 %, 49.1 ± 4.8 %, 54.1 ± 5.2 % and 55.7 ± 4.0 % in RA, RB, RC and RD respectively. The microbiome assembly process in CK was extremely slow due to the absence of initial microbes with the low average NH_4^+-N removal efficiency of 11.4 ± 12.9 %. All microbiomes exhibited similar metabolic characteristics of nitrogen assimilation without inorganic intermediates accumulation. Considering the empirical C/N ratio of 20 for the heterotrophic metabolism (Winkler and Straka 2019), the C/N ratio of synthetic wastewater was then optimized to 20 for better nitrogen removal performance in heterotrophic microbiome after 30 days (Zhang et al., 2022). All microbiomes subsequently demonstrated significant improvements in NH_4^+-N efficiencies. Compared with RA and RB, microbiomes with multiple microbes as the initial functional microbes showed superior performance in RC and RD. During the whole operation, the accumulation of neither nitrite nor nitrate was observed in all bioreactors with the average NO_2^--N and NO_3^--N concentrations as low as 0.53 ± 0.40 mg/L and 0.11 ± 0.10 mg/L (Fig. 4b and c). Average NH_4^+-N efficiencies in the stable operation phase were stable at levels as high as 76.0 ± 4.1 %, 76.2 ± 4.4 %, 92.2 ± 1.2 % and 90.8 ± 3.1 % in RA, RB, RC and RD, respectively (Fig. 4d). Due to negligible nitrite and nitrate accumulation, efficient TN removal performance was achieved in heterotrophic microbiomes with the average efficiencies of 72.0 ± 4.7 % (RA), 72.2 ± 5.0 % (RB), 86.4 ± 5.4 % (RC) and 87.0 ± 4.1 % (RD) (Fig. 4e). By comparison, CK exhibited prolonged acclimatization with significantly higher residual NH_4^+-N in effluent. The average NH_4^+-N and TN removal efficiencies in CK were also as low as 35.9 ± 12.9 % and 34.9 ± 7.50 % respectively, reflecting the relatively weaker ammonium removal capability of the environmental microbiota compared to HN-AD functional strains.

The nitrogen metabolism batch test revealed the ammonium-assimilating nitrogen transformation of microbiomes under different C/N ratios from 5 to 20 (Fig. S4, Fig. S5 and Fig. S6). Under the C/N ratio of 20 (Fig. S4), four microbiomes performed efficient ammonium transformation capabilities. The stable total nitrogen in all systems without significant gaseous nitrogen escaping from the solution during ammonium removal under different C/N ratios suggested the complete assimilation of supernatant TN into biomass even at low C/N ratios. Consequently, all microbiomes removed ammonium through ammonium assimilation rather than gaseous nitrogen production through nitrification (Zhang et al., 2021).

3.3.2. Sludge properties

The initially elevated turbidity values in effluent of each microbiomes revealed the free-living and uncolonized environmental microbes at the start-up phase (Fig. 4f). Turbidity gradually decreased in all reactors during the process of microbiome assembly. When matured microbiomes were constructed, CK undoubtedly exhibited the highest turbidity of 14.7 NTU. The lower turbidity at the start-up phase in RA, RC and RD than CK revealed the better settleability of microbial flocs and aggregating role of strain 8-C and A4N01 in microbiome construction. Sludge biomass accumulation showed that fillers in RB enhanced the biomass proliferation (Fig. S3). The accumulation of biomass in reactors ensured efficient nitrogen removal (Zhang et al., 2022), but the lower biomass in RB resulted in the lower nitrogen removal performance than other reactors (Fig. S3). Interestingly, RB and RC showed the lowest turbidity of 3.0 and 6.8 NTU, respectively. The content of proteins (PN)

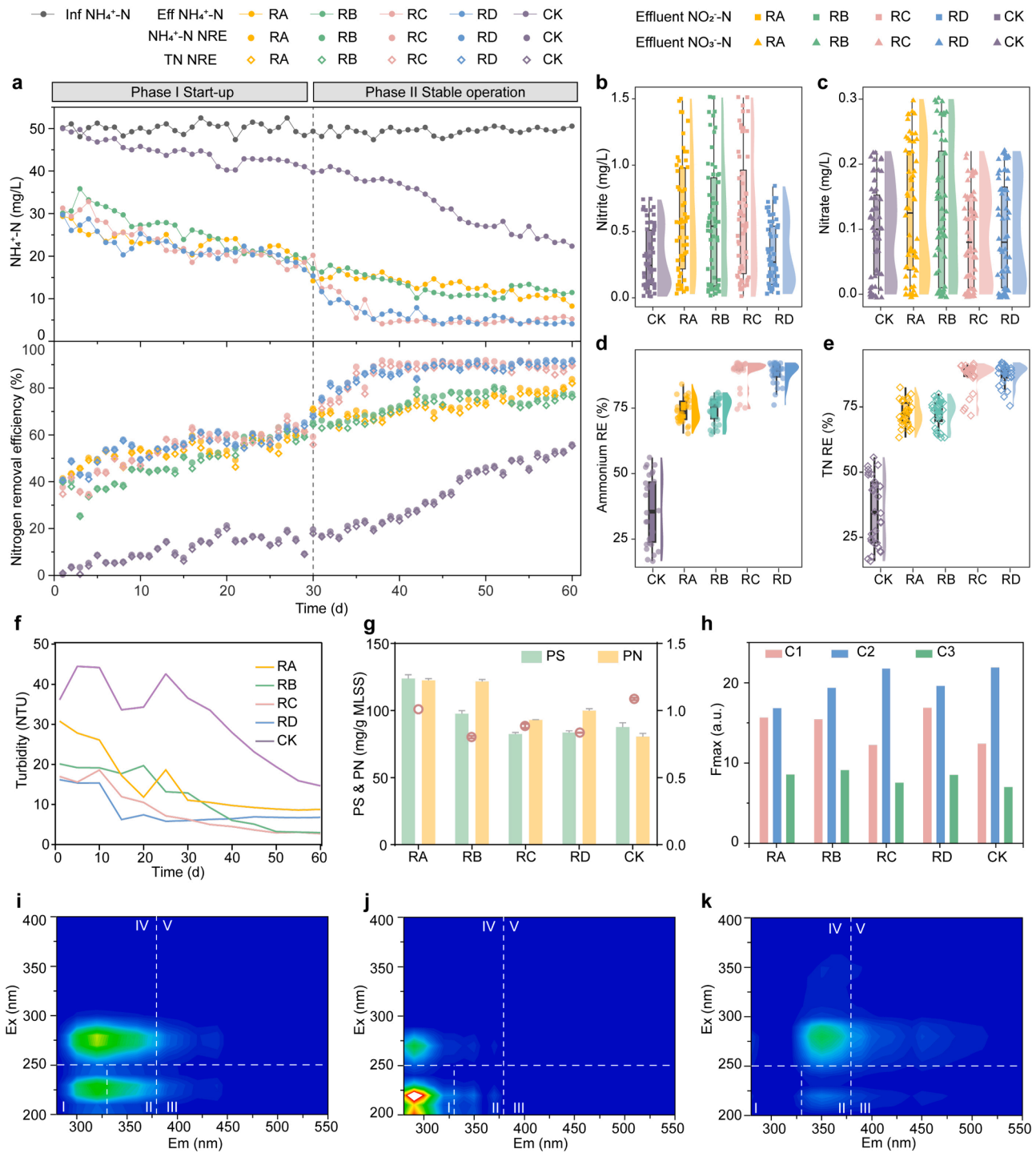

Fig. 4. The performance of nitrogen removal and characterization of sludge in bioreactors. a, Ammonium removal performance and nitrogen removal efficiency. b, Nitrite concentration. c, Nitrate concentration. d, Ammonium removal efficiencies. e, Total nitrogen (TN) removal efficiencies. f, Turbidity of effluent. g, Concentrations of polysaccharide (PS) and protein (PN) in extracellular polymeric substance (EPS). h, The Fmax of three main fluorescence components - component 1 (C1), component 2 (C2), and component 3 (C3) in EPS. i-k, The main fluorescence component C1(i), C2 (j) and C3(k) of EPS in sludge from different reactors.

and polysaccharide (PS) in EPS explained the differences of turbidity among microbiomes (Fig. 4g). RA exhibited the highest polysaccharide (PS) and protein (PN) concentrations yet maintained a PS/PN ratio >1, indicating the hydrophilicity of EPS which probably increased effluent turbidity. In CK, the consistently low EPS production yet the relatively high PS/PN ratio suggested difficulties for free-living environmental microbes to colonize during the formation of biofilms.

Three-dimensional excitation-emission matrix (3D-EEM) fluorescence spectroscopy was employed to characterize EPS (Fig. 4h-k). Component 1 displayed two major peaks at excitation/emission (Ex/Em) wavelengths of 270–280/300–350 nm and 210–230/300–350 nm corresponding to proteins containing tyrosine and tryptophan, as well as soluble microbial byproduct-like materials (Jiang et al., 2024). Component 2 exhibited protein-like peak at 260/275 nm in region IV and tyrosine-like fluorescence peak at 220/275 nm in region I. Component 3 revealed two prominent peaks at 275/350 nm (tryptophan) and 230/350 nm (aromatic proteins). The characteristics of EPS components confirmed the protein-dominated EPS composition with

few humic acids in all heterotrophic microbiomes. The protein-rich EPS composition, particularly abundant hydrophobic protein groups, enhanced the biofilm formation and sludge aggregation during microbiome construction (Han et al., 2024).

3.4. Microbial communities and bacterial interactions

3.4.1. Microbial diversity and bacterial community structure

Temporal changes in microbial diversity and richness of bacterial communities were assessed (Fig. 5a). Index values of both species richness and diversity showed significantly increase and stabilized at relatively high levels at the end of construction (Table S7). There was no statistically significant difference in species richness among the five microbiomes, but RB exhibited significantly higher Shannon index values compared to other microbiomes (Fig. S7), probably due to diverse ecological niches provided by biofilms (Li et al., 2025). Venn diagram analysis and NMDS analysis demonstrated the coexistence of both shared and unique OTUs among microbiomes, while each microbiome established distinct bacterial community structure (Fig. 5b-c). A total of 97 OTUs were shared in five systems, indicating that most of the microbes involved in microbiome assembly were derived from the environment.

Time series of microbial structures revealed the assembly of bacterial interactions between the applied strain and environmental microbes in microbiomes (Fig. S8). The initial microbes were replaced by large numbers of environmental microbes within 10 days, while all microbiomes developed mature and stable microbial community structure after 30 days. Finally, the bacterial phyla were dominated by *Proteobacteria* and *Bacteroidota*, accounting for approximately 99 % of total relative abundances. At the genus level, abundances of initial strains decreased rapidly. In RA, abundances of *Pseudomonas* remained at 85 % after 5 days yet decreased to 0.4 %, 0.1 %, 0.1 % and 0.1 % at 10, 30, 50 and 60 days, respectively. In RB, microbial community changed tremendously at the 5 days, probably due to the rapid community succession that occurred during the process of microbial colonization on fillers. As a result, the average abundance of *Acinetobacter* was 0.004 %

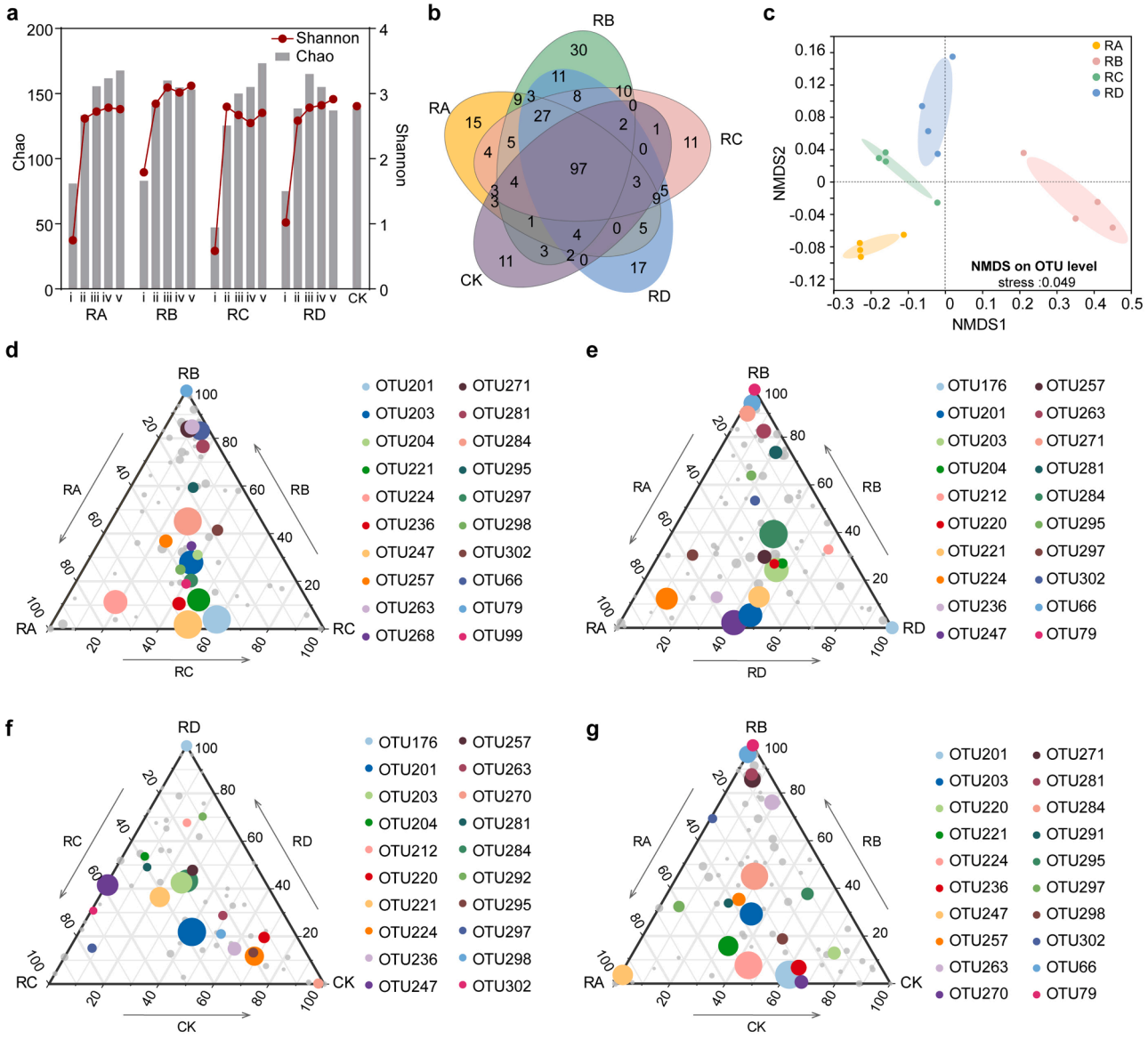

Fig. 5. Bacterial diversity and bacterial community compositional structure. a, Bacterial diversity and richness represented by indexes Chao and Shannon. b, Venn diagrams of unique and shared bacterial OTU among five microbiomes (RA, RB, RC, RD and CK). c, Bacterial community compositional structure indicated by non-metric multidimensional scaling (NMDS) plots. d-g, Ternary plots of bacterial OTU distribution in different microbiomes. The size of the circles represented the mean relative abundance of bacterial OTU.

in RB. Although two functional strains were added into RC with a ratio of 1:1, the abundance of *Acinetobacter* decreased rapidly to an undetectable abundance, whereas *Pseudomonas* maintained a relatively high abundance (87.11 %). In RD, a similar pattern emerged that abundances of *Psychrobacter* (which strain A4N01 belonged to) in RD decreased from 31.1 % at the start-up phase to 0.014 % after 10-day operation, and remained at an extremely low level (0.004–0.009 %). The more effective maintenance of strain 8-C and strain A4N01 in the microbiome was probably attributed to the settling capability of their floc-like biofilms. Nevertheless, the increasing diversity and the decreasing abundance of functional microbes did not significantly affect the nutrient removal performances of the HN-AD system, which can be explained by the theory of keystone taxa (Zhang et al., 2021). Specifically, keystone taxa could drive the function of microbial consortia despite their low abundance by recruiting similar functional environmental microbes (Banerjee et al., 2018).

Ternary map visualized the distinct enrichment patterns of bacterial communities over microbiomes constructed derived from specific functional microbes (Fig. 5d-g). In RA, bacterial groups were significantly enriched in *Nitratireductor* (OTU224), *Pseudomonas* (OTU247) and SM1A02 (OTU297). In RB, genera *Halomonas* (OTU281, OTU79), *Gemmobacter* (OTU66) and *Bacillus* (OTU99) were enriched. The bacterial consortia of RC and RD integrated the characteristics of microbial communities in both RA and RB, as well as CK. LEfSe analysis demonstrated that functional microbes enriched different environmental microbes as biomarkers in microbiomes, resulting in distinct microbial community structure (Fig. S9). Genus *Nitratireductor* (23.6 %) and TM7a (3.3 %) were detected as biomarkers with significantly abundant (>1 %) in RA. Genus *Xanthomarina* (19.4 %), *Vitellibacter* (11.9 %), *Halomonas* (10.5 %) and *Nautella* (8.9 %) were the biomarker in RB. Genus *Planktosalinus* (26 %) and *Stappia* (14.1 %) were biomarkers in RC. Genus *Paracoccus* (2.3 %), *Lacimicrobium* (2.3 %), *Gelidibacter* (0.6 %) and *Marinicella* (0.03 %) were in RD. Remarkably, these biomarkers were frequently identified as heterotrophs in saline wastewater treatment biosystems with high organic loading (Corsino et al., 2019), while representative ammonia-oxidizing bacteria (AOB) and nitrite-oxidizing bacteria (NOB) were not detected in all microbiomes. The prediction of nitrogen metabolic genes also confirmed the absent of nitrification in heterotrophic microbiomes (Fig. S10).

3.4.2. Bacterial interactions and assembly of microbiomes

Co-occurrence networks revealed the microbial interactions in heterotrophic microbiomes (Fig. 6a-d). Positive associations (> 60 %) predominated all networks, suggesting cooperative relationships among microbes. These four heterotrophic microbiomes sharing the similar nitrogen function exhibited comparable topological structures with modular structures, evidenced by modularity index exceeding 0.7 (Table S8). All keystone taxa across four microbiomes were identified as connectors by classifying network nodes based on analysis of within modular degree and between modular degree (Fig. 6e-h). RA (number of

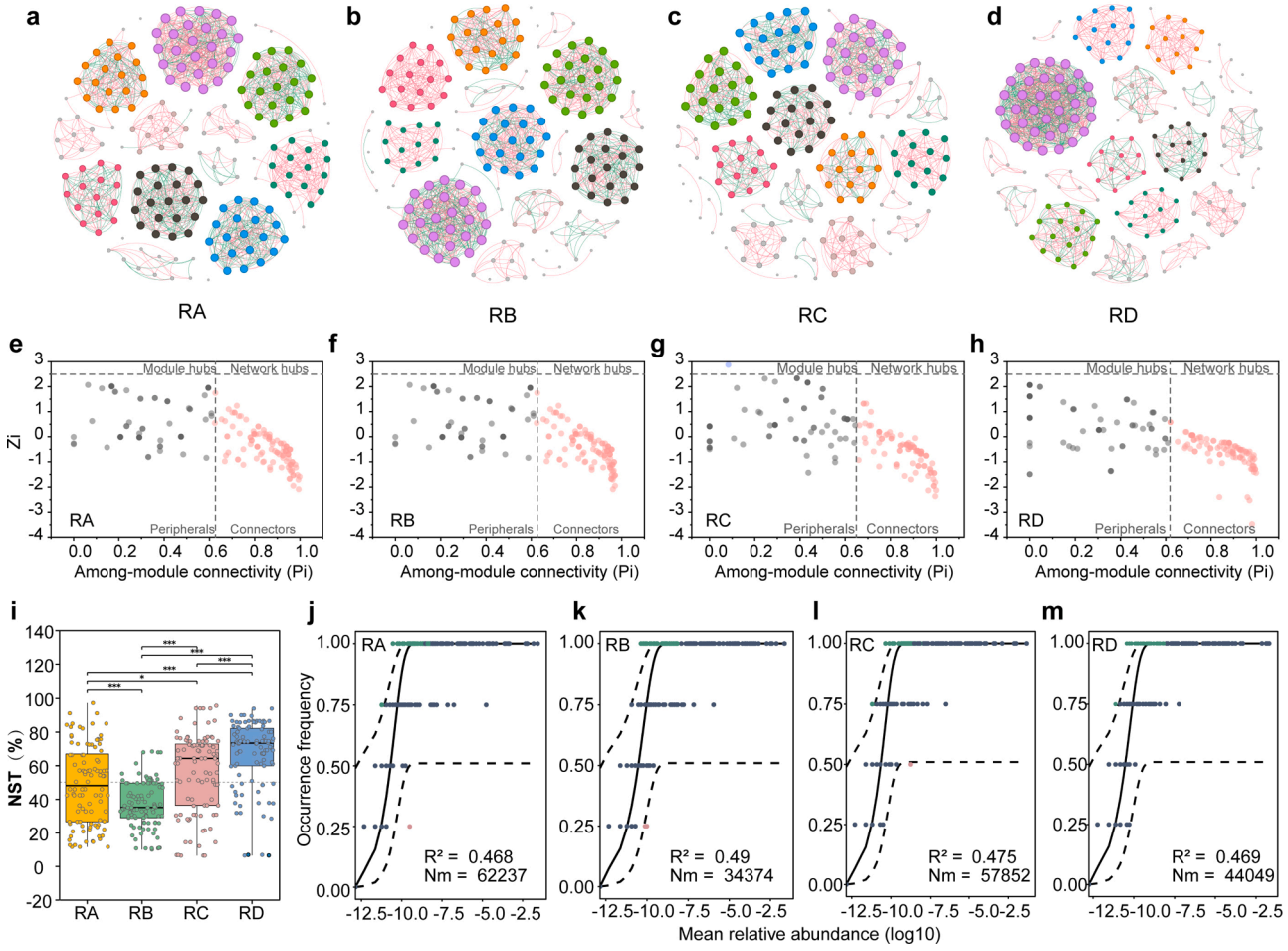

Fig. 6. Bacterial co-occurrence networks and community assembly. a-d, Bacterial cooccurrence networks of five microbiomes. e-h, Identification of keystone taxa in microbial community based on Zi Pi. Threshold values of within-module connectivity (Zi) and amongmodule connectivity (Pi) for categorizing bacterial OTUs are 2.5 and 0.62, respectively. i, NST analysis of heterotrophic microbiomes in bacterial community assembly. j-m, Fit of the neutral community model (NCM) of community assembly. Nm and R2 indicated the immigration rate and the fit to this model, respectively. The relative abundance of three categories of OTUs (above prediction, below prediction, and neutrally distributed) in bacterial communities were showed at the corner of each figure.

109) and RB (number of 117) contained more keystone taxa, demonstrating higher connectivity among modules. RC and RD, by contrast, displayed stronger internal interactions in modules and weaker external connectivity. As expected, HN-AD functional microbes *Pseudomonas* and *Acinetobacter* were identified as the keystone taxa in RA and RB. Notably, while *Pseudomonas* was indicated as keystone taxa in RC or RD, *Acinetobacter* was absent probably because of its poor capability of biomass retention. The genus *Psychrobacter* was also identified as keystone taxon in RD, confirming the key role of biofilm-forming microbes in the process of microbiome construction. Furthermore, the relative abundance of genes related to acyl-homoserine lactone (AHL)-mediated quorum sensing (QS) showed significant increase during microbiome assembly (Fig. S11), demonstrating the possible regulation of QS in biofilm formation.

Normalized stochasticity ratio (NST) was further employed to quantify the role of deterministic and stochastic processes in microbiome assembly (Fig. 6i). The NST values of RA and RB were below the 50 % boundary, indicating more important role of deterministic process than the stochasticity during microbial assembly (Ning et al., 2019). Conversely, stochastic processes might play more important role in community assembly of RC and RD with higher NST values. The neutral model (NCM) was used to evaluate the fit of neutral processes such as birth, death, and immigration in explaining microbial community assembly patterns (Fig. 6j-m). Unfortunately, the relatively low R^2 values (<0.5) in NCM results revealed that stochasticity played minor role in microbial community shaping. Consequently, the deterministic process overall dominated bacterial community assembly patterns in these synthetic microbiomes, which contributed to the predictable results and stable function in microbiome construction.

4. Discussion

In this study, the HN-AD capability of pure-cultured functional microbes has been proven under saline environments and various conditions. The proportion of heterotrophic nitrogen assimilation usually accounts for approximately half and even higher flux (Deng et al., 2021; Wang and He 2020), suggesting the crucial role of ammonium assimilation in saline BNR. Interestingly, the heterotrophic nitrification process has been completely suppressed by ammonium assimilation in microbial communities even at low C/N ratio. Consequently, these synthetic microbiomes established by HN-AD functional strains should be defined as heterotrophic ammonium-assimilating microbiomes (Fig. 7).

Time-series abundances of nitrogen functional genes in these microbiomes (Fig. S12) verified that ammonium assimilation dominated nitrogen metabolism and was enhanced during microbiome construction, confirmed by the relatively high abundances of *glnA*. In RD, the abundance of *glnA* showed the highest level at the set-up phase, indicating the addition of ammonium-assimilating strain A4N01. Considering the abundance of A4N01 was dropped to an extremely low level, the high abundances of *glnA* in all microbiomes were contributed by environmental microbes with ammonium-assimilating capability. Although the control microbiome was composed of environmental microbes also existing in other microbiomes, the obviously lower nitrogen metabolism in CK indicated the crucial role of the initial microorganisms in start-up phase. The microbial nitrogen metabolism fluxes were quantitatively dominated by ammonium assimilation in natural environment (Kuypers et al., 2018), explaining the easy enrichment of ammonium-assimilating environmental microbes. Therefore, the crucial role played by HN-AD microbes, as keystone taxa, lied in the selective recruitment of ammonium-assimilating microbes with efficient competitive ability for nitrogen substrates at the start-up phase of microbiome assembly.

In view of nitrification, the extremely low abundances of nitrifying functional genes (*amoA* and *nxrA*) revealed the absent of autotrophic AOB in microbiomes. Our previous results confirmed the difficulty of enriching autotrophic nitrifiers under saline conditions in microbial consortia (Zhang et al., 2021). Autotrophic AOB exhibit slow growth rate because of their limited electron availability for biosynthesis (Wu et al., 2024), and consequently hardly compete with heterotrophic microbes with better tolerance to adverse conditions, higher growth rate and easier enrichment in microbiomes. The detection of heterotrophic nitrification biomarkers (*haoA, haoB* and *haoC*) and aerobic denitrification biomarker (*napA*) in microbiomes revealed the presence of HN-AD bacteria in microbiomes (Fig. S12). Yet, abundance of HN-AD functional microorganisms continuously decreased due to the invasion of the environmental microbes during the competitive interactions between HN-AD strains and environmental microbes in community assembly, confirmed by the decreasing abundances of *napA* and increasing Ct value of *haoA*. Simultaneously, the enrichment ammonium-assimilating microbes finally led to the result that the heterotrophic nitrification was suppressed by ammonium assimilation during the competitive interactions between HN-AD strains and environmental microbes in community assembly. This inevitable invasion of environmental microbes in the process of biofilm formation could not guaranteed the metabolic function, especially functional microbes without unique ecological niche.

Nitrogen assimilation has been oversimplified as the heterotrophic nitrification process in previous studies. The dependence of aerobic ammonium removal on organic carbon is commonly regarded as a criterion for identifying heterotrophic nitrification. Yet, nitrogen assimilation represents another aerobic and heterotrophic transformation pathway. Since HN-AD bacteria are prevalent in saline conditions than in freshwater systems (Sui et al., 2024), the nitrogen metabolism of

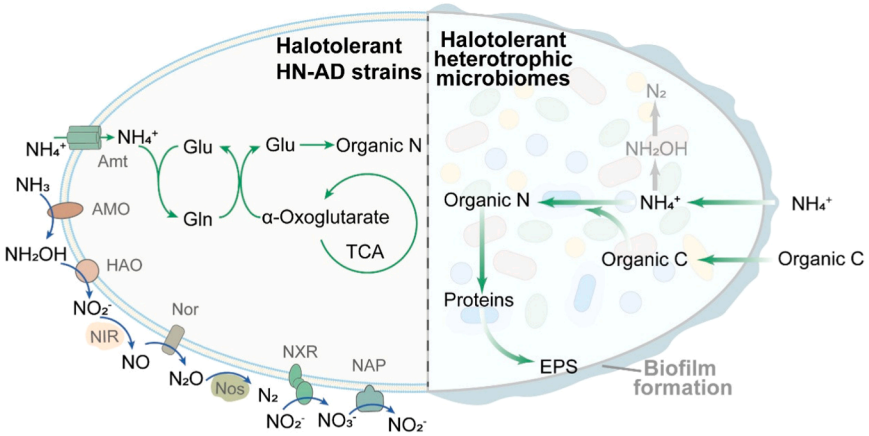

Fig. 7. Schematic diagram of halotolerant nitrogen metabolism in pure-cultured HN-AD strains and heterotrophic microbiomes. Glu, glutamic acid; Gln, glutamine.

halophilic microbiomes containing or constructed by HN-AD bacteria are generally defined as HN-AD (Pan et al., 2020) without further distinction between heterotrophic nitrification and assimilation. Therefore, we highlight that the heterotrophic nitrogen assimilation plays an even larger role given the microbial community complexity, and likely constitutes the primary nitrogen removal mechanism in saline wastewater treatment.

Constructing microbiomes with functional bacteria offers a novel and promising strategy for saline wastewater treatment. Biofilm formation serves as a critical process enabling the development of complex microbial communities and ultimately ensuring community stability (Afonso et al., 2021; Afonso et al., 2025), and heterotrophic auto-aggregating bacteria have been successfully applied to effective nitrogen removal by promoting granulation or colonization (Zhang et al., 2024). Our results reaffirm the pivotal role of biofilm-forming microbes in synthetic microbiome construction, especially at the startup stage of rapid enrichment of microbes. The protein secretion in EPS during biofilm formation could enhance the proliferation of functional microbes (Afonso et al., 2025). Thus, strategies for stimulating EPS and protein secretion, such as adding quorum-sensing signaling molecules and promoting C/N ratio, could enhance biofilm formation and resultant proliferation of functional microbes (Zhang et al., 2021). Our study proposes a promising strategy for applying functional HN-AD microorganisms to BNR in saline wastewater - a cost-effective solution with technological and economic advantages. From the perspective of future engineering applications, regulatory strategy for optimizing microbiome construction still holds significant research potential.

5. Conclusions

(1) Two novel halophilic HN-AD strains with effective metabolism in various conditions, *Pseudomonas kunmingens* 8-C and *Acinetobacter johnsonii* 2–1-H, were isolated, and the strain 8-C showed auto-aggregating capability.

(2) The nitrogen removal pathways of two strains were classified into assimilation from NH_4^+-N to biomass and HN-AD speculated as NH_4^+-N→NH_2OH→NO→N_2O→N_2 or NH_4^+-N→NH_2OH→NO_2^--N→NO_3^--N→NO_2^--N→NO→N_2O→N_2. Approximately half of the ammonium was removed through assimilation in process of heterotrophic nitrification, while aerobic denitrification accounted for as high as 68–75 % nitrate removal.

(3) Four heterotrophic ammonium-assimilating microbiomes were constructed by HN-AD strains and auto-aggregating strains. These microbiomes showed shorter start-up phase, better sludge properties and higher nitrogen removal performance than the control with average ammonium and TN removal efficiencies higher than 76 % and 70 %.

(4) The initial functional microbes played key role in recruiting efficient ammonium-assimilating microbes and shaping distinct microbial consortia through the deterministic process. The nitrogen function of ammonium assimilation carried out by enriched environmental microbes completely suppressed nitrification of HN-AD bacteria in microbiomes.

CRediT authorship contribution statement

Mengru Zhang: Writing – review & editing, Writing – original draft, Visualization, Funding acquisition, Data curation. **Wenhao Zhang:** Formal analysis, Data curation. **Qingyuan Jiang:** Data curation. **Chuanfu Zhao:** Visualization. **Fei Han:** Writing – review & editing. **Hao Chen:** Writing – original draft. **Yuke Li:** Writing – review & editing. **Yuping Zhuge:** Writing – review & editing. **Weizhi Zhou:** Writing – review & editing, Supervision, Methodology, Funding acquisition.

Declaration of competing interest

The authors declare that they have no known competing financial interests or personal relationships that could have appeared to influence the work reported in this paper.

Acknowledgment

This work was supported by National Natural Science Foundation of China (52300097); Natural Science Foundation of Shandong Province (ZR2023QE180); National Key R&D Program of China (2022YFC2807503); China Postdoctoral Science Foundation (2023M732061).

Supplementary materials

Supplementary material associated with this article can be found, in the online version, at doi:10.1016/j.watres.2025.124694.

Data availability

All 16S rRNA gene sequencing data of microbiome samples are deposited into the GenBank SRA database in BioSample SAMN49264178 - SAMN49264198 under BioProject PRJNA1278807.

References

Afonso, A.C., Gomes, I.B., Saavedra, M.J., Giaouris, E., Simões, L.C., Simões, M., 2021. Bacterial coaggregation in aquatic systems. Water Res. 196, 117037.
Afonso, A.C., Saavedra, M.J., Simões, M., Simões, L.C., 2025. The role of the proteosurfaceome and exoproteome in bacterial coaggregation. Biotechnol. Adv. 79, 108505.
Banerjee, S., Schlaeppi, K., van der Heijden, M.G.A., 2018. Keystone taxa as drivers of microbiome structure and functioning. Nat. Rev. Microbiol. 16 (9), 567–576.
Corsino, S.F., Capodici, M., Di Pippo, F., Tandoi, V., Torregrossa, M., 2019. Comparison between kinetics of autochthonous marine bacteria in activated sludge and granular sludge systems at different salinity and SRTs. Water Res. 148, 425–437.
Cui, Y., Cui, Y.-W., Huang, J.-L., 2021. A novel halophilic exiguobacterium mexicanum strain removes nitrogen from saline wastewater via heterotrophic nitrification and aerobic denitrification. Bioresour. Technol. 333, 125189.
Deng, M., Zhao, X., Senbati, Y., Song, K., He, X., 2021. Nitrogen removal by heterotrophic nitrifying and aerobic denitrifying bacterium Pseudomonas sp. DM02: removal performance, mechanism and immobilized application for real aquaculture wastewater treatment. Bioresour. Technol. 322, 124555.
Denk, T.R.A., Mohn, J., Decock, C., Lewicka-Szczebak, D., Harris, E., Butterbach-Bahl, K., Kiese, R., Wolf, B., 2017. The nitrogen cycle: a review of isotope effects and isotope modeling approaches. Soil Biol. Biochem. 105, 121–137.
DuBois, M., Gilles, K.A., Hamilton, J.K., Rebers, P.A., Smith, F., 1956. Colorimetric method for determination of sugars and related substances. Anal. Chem. 28 (3), 350–356.
Han, N.-N., Yang, J.-H., Fan, N.-S., Jin, R.-C., 2024. Mechanistic insight into microbial interaction and metabolic pattern of anammox consortia on surface-modified biofilm carrier with extracellular polymeric substances. Bioresour. Technol. 407, 131092.
Hu, J., Tian, J., Deng, X., Liu, X., Zhou, F., Yu, J., Chi, R., Xiao, C., 2024. Heterotrophic nitrification processes driven by glucose and sodium acetate: new insights into microbial communities, functional genes and nitrogen metabolism from metagenomics and metabolomics. Bioresour. Technol. 408, 131226.
Huang, F., Pan, L., He, Z., Zhang, M., Zhang, M., 2020. Identification, interactions, nitrogen removal pathways and performances of culturable heterotrophic nitrification-aerobic denitrification bacteria from mariculture water by using cell culture and metagenomics. Sci. Total Environ. 732, 139268.
Huang, M.-Q., Cui, Y.-W., Yang, H.-J., Xu, M.-J., Cui, Y., Chen, Z., 2023. A halophilic aerobic-heterotrophic strain Halomonas venusta SND-01: nitrogen removal by ammonium assimilation and heterotrophic nitrification-aerobic denitrification. Bioresour. Technol. 374, 128758.
Huang, Z., Wang, Y., Jiang, L., Xu, B., Wang, Y., Zhao, H., Zhou, W., 2018. Mechanism and performance of a self-flocculating marine bacterium in saline wastewater treatment. Chem. Eng. J. 334, 732–740.
Jiang, K., Gao, Q., Feng, J., Zhu, S., Zhai, W., Wu, D., Zhang, H., Zhang, W., Liu, X., Zhang, J., Wang, S., Wang, Z., 2024. Impact of phenolic-formaldehyde resin microplastics on anaerobic granular sludge: EPS interaction mechanisms and impacts on reactor performance. J. Hazard. Mater. 480, 136308.
Ke, X., Wu, Z.-D., Zhang, X.-Y., Zhou, S.-p., Zhang, Y.-C., Xue, Y.-p., Zheng, Y.-G., 2025. Nitrogen removal characteristics and salt tolerance mechanisms of the novel bacterium Halomonas sp. W07 in saline wastewater treatment. Bioresour. Technol. 426, 132338.
Kuypers, M.M.M., Marchant, H.K., Kartal, B., 2018. The microbial nitrogen-cycling network. Nat. Rev. Microbiol. 16 (5), 263–276.

Lan, M., Yin, Q., Wang, J., Li, M., Li, Y., Li, B., 2023. Heterotrophic nitrification-aerobic denitrification performance of a novel strain, Pseudomonas sp. B-1, isolated from membrane aerated biofilm reactor. Environ. Res. 220, 115199.
Lawson, C.E., Harcombe, W.R., Hatzenpichler, R., Lindemann, S.R., Löffler, F.E., O'Malley, M.A., García Martín, H., Pfleger, B.F., Raskin, L., Venturelli, O.S., Weissbrodt, D.G., Noguera, D.R., McMahon, K.D., 2019. Common principles and best practices for engineering microbiomes. Nat. Rev. Microbiol. 17 (12), 725–741.
Lenferink, W.B., Bakken, L.R., Jetten, M.S.M., van Kessel, M.A.H.J., Lücker, S., 2024. Hydroxylamine production by Alcaligenes faecalis challenges the paradigm of heterotrophic nitrification. Sci. Adv. 10 (23), eadl3587.
Li, J., Wang, H., Li, Z., Xie, J., Tsybekmitova, G.T., Wang, Y., 2025. Membrane aeration accelerated nitrifying biofilm formation and optimized spatial niche differentiation in aerobic biofilm-based reactors for enhanced nitrogen removals. Chem. Eng. J. 506, 160297.
Li, Y.-y., Lin, L., Huang, X., Li, X.-y, 2023. Partial nitritation-anammox for treatment of saline wastewater: hydrazine-assisted salinity adaptation and nitrate control. Chem. Eng. J. 470, 144268.
Lowry, O., Rosebrough, N., Farr, A.L., Randall, R., 1951. Protein measurement with the folin phenol reagent. J. Biol. Chem. 193 (1), 265–275.
Mariotti, A., 1983. Atmospheric nitrogen is a reliable standard for natural 15N abundance measurements. Nature 303 (5919), 685–687.
Martikainen, P.J., 2022. Heterotrophic nitrification – An eternal mystery in the nitrogen cycle. Soil Biol. Biochem. 168, 108611.
Ning, D., Deng, Y., Tiedje, J.M., Zhou, J., 2019. A general framework for quantitatively assessing ecological stochasticity. Proc. Natl. Acad. Sci. 116 (34), 16892–16898.
Pan, Z., Zhou, J., Lin, Z., Wang, Y., Zhao, P., Zhou, J., Liu, S., He, X., 2020. Effects of COD/TN ratio on nitrogen removal efficiency, microbial community for high saline wastewater treatment based on heterotrophic nitrification-aerobic denitrification process. Bioresour. Technol. 301, 122726.
Qiang, L., Yunlong, W., Chisheng, Y., Ancheng, L., Zhiwei, L., 2023. New insights into differential salinity tolerance between autotrophic and heterotrophic partial nitrification. J. Environ. Chem. Eng. 11 (3), 109681.
Ren, J., Cheng, X., Ma, H., Ma, X., 2021. Characteristics of a novel heterotrophic nitrification and aerobic denitrification bacterium and its bioaugmentation performance in a membrane bioreactor. Bioresour. Technol. 342, 125908.
Ruan, Z., Chen, K., Cao, W., Meng, L., Yang, B., Xu, M., Xing, Y., Li, P., Freilich, S., Chen, C., Gao, Y., Jiang, J., Xu, X., 2024. Engineering natural microbiomes toward enhanced bioremediation by microbiome modeling. Nat. Commun. 15 (1), 4694.
Shi, K., Xu, J.-M., Cui, H.-L., Cheng, H.-Y., Liang, B., Wang, A.-J., 2024. Microbiome regulation for sustainable wastewater treatment. Biotechnol. Adv. 77, 108458.
Srivastava, A., Parida, V.K., Majumder, A., Gupta, B., Gupta, A.K., 2021. Treatment of saline wastewater using physicochemical, biological, and hybrid processes: insights into inhibition mechanisms, treatment efficiencies and performance enhancement. J. Environ. Chem. Eng. 9 (4), 105775.
Sui, Y., Cui, Y.-W., Huang, J.-L., Xu, M.-J., 2024. Feast/famine ratio regulates the succession of heterotrophic nitrification-aerobic denitrification and autotrophic ammonia oxidizing bacteria in halophilic aerobic granular sludge treating saline wastewater. Bioresour. Technol. 393, 129995.
Wang, Q., He, J., 2020. Complete nitrogen removal via simultaneous nitrification and denitrification by a novel phosphate accumulating thauera sp. strain SND5. Water Res. 185, 116300.
Wei, X., Li, S., Li, C., Liao, J., Yang, Y., He, Z., Dong, K., Lee, S.-S., 2025. Characterization and genomic insights into the nitrogen metabolism of heterotrophic nitrifying and aerobic denitrifying bacterium Pseudomonas aeruginosa WS-03. J. Environ. Manag. 376, 124405.
Winkler, M.K., Straka, L., 2019. New directions in biological nitrogen removal and recovery from wastewater. Curr. Opin. Biotechnol. 57, 50–55.
Wu, Y., Cui, Y., Li, D., Yin, M., Pei, Y., Wang, X., Li, J., Zhu, Y., 2024. Fulvic acid mediated highly efficient heterotrophic nitrification-aerobic denitrification by Paracoccus denitrificans XW11 with reduced C/N ratio. Water Res. 267, 122557.
Xi, H., Zhou, X., Arslan, M., Luo, Z., Wei, J., Wu, Z., Gamal El-Din, M., 2022. Heterotrophic nitrification and aerobic denitrification process: promising but a long way to go in the wastewater treatment. Sci. Total Environ. 805, 150212.
Xie, Y., Tian, X., He, Y., Dong, S., zhao, K., 2023. Nitrogen removal capability and mechanism of a novel heterotrophic nitrification–aerobic denitrification bacterium Halomonas sp. DN3. Bioresour. Technol. 387, 129569.
Xu, M.-J., Cui, Y.-W., Huang, M.-Q., Sui, Y., 2024. Simultaneous inorganic nitrogen and phosphate removal by aerobic-heterotrophic fungus fusarium keratoplasticum FSP1: performance, pathway and application. Bioresour. Technol. 393, 130141.
Xu, R.-Z., Cao, J.-S., Cheng, S., Luo, J.-Y., Ni, B.-J., Fang, F., Liu, W., Wang, P., 2025. Heterotrophic nitrification-aerobic denitrification strains: an overlooked microbial interaction nexus in the anaerobic-swing-anoxic-oxic (ASAO) plug-flow system. J. Environ. Manage. 380, 125030.
Yang, R.-c., Cui, Y.-w., Li, Z.-y., Li, M.-t., Jiang, L.-x., Mi, Y.-n., Sui, Y., Liang, H.-k, 2025. Molecular identification of heterotrophic nitrification and aerobic denitrification bacteria: from methods development to application demonstration. Water Res. 280, 123542.
Zhang, M., Han, F., Li, Y., Liu, Z., Chen, H., Li, Z., Li, Q., Zhou, W., 2021. Nitrogen recovery by a halophilic ammonium-assimilating microbiome: a new strategy for saline wastewater treatment. Water Res., 117832
Zhang, M., Han, F., Liu, Z., Han, Y., Li, Y., Zhou, W., 2022. Ammonium-assimilating microbiome: a halophilic biosystem rationally optimized by carbon to nitrogen ratios with stable nitrogen conversion and microbial structure. Bioresour. Technol. 350, 126911.
Zhang, S., Sun, X., Fan, Y., Qiu, T., Gao, M., Wang, X., 2017. Heterotrophic nitrification and aerobic denitrification by Diaphorobacter polyhydroxybutyrativorans SL-205 using poly(3-hydroxybutyrate-co-3-hydroxyvalerate) as the sole carbon source. Bioresour. Technol. 241, 500–507.
Zhang, W., Cao, B., Wang, D., Ma, T., Xia, H., Yu, D., 2016. Influence of wastewater sludge treatment using combined peroxyacetic acid oxidation and inorganic coagulants re-flocculation on characteristics of extracellular polymeric substances (EPS). Water Res. 88, 728–739.
Zhang, Y., Sang, P., Wang, K., Gao, J., Liu, Q., Wang, J., Qian, F., Shu, Y., Hong, P., 2024. Enhanced chromium and nitrogen removal by constructing a biofilm reaction system based on denitrifying bacteria preferential colonization theory. Ecotoxicol. Environ. Saf. 273, 116156.
Zhao, C., Lei, J., Han, F., Jiao, T., Han, Y., Zhou, W., 2023. Novel strategy for treating high salinity oilfield produced water: pyrite-activated peroxymonosulfate coupled with heterotrophic ammonia assimilation. Water Res. 247, 120772.